

Bounding Uncertainty in EKF-SLAM: The Robocentric Local Approach

Ruben Martinez-Cantin José A. Castellanos

*Dept. Informática e Ingeniería de Sistemas
Instituto de Investigación en Ingeniería de Aragón (I3A)
Universidad de Zaragoza
María de Luna 1, E-50018 Zaragoza, Spain
Email: {rmcantin, jacaste}@unizar.es*

Abstract—This paper addresses the consistency issue of the Extended Kalman Filter approach to the simultaneous localization and mapping (EKF-SLAM) problem. Linearization of the inherent nonlinearities of both the motion and the sensor models frequently drives the solution of the EKF-SLAM out of consistency specially in those situations where location uncertainty surpasses a certain threshold. This paper proposes a robocentric local map sequencing algorithm which: (a) bounds location uncertainty within each local map, (b) reduces the computational cost up to constant time in the majority of updates and (c) improves linearization accuracy by updating the map with sensor uncertainty level constraints. Simulation and large-scale outdoor experiments validate the proposed approach.

I. INTRODUCTION

Probabilistic simultaneous localization and mapping (SLAM) has become a milestone in mobile robotics literature. By definition, it is the problem to determine the position and heading of a vehicle moving through an unknown environment and, concurrently, to learn useful information from the surroundings taking into account sensor errors.

The first approximation to probabilistic SLAM, dates back to the seminal work of Smith et al. [1], where a discrete-time state-space framework, named the *stochastic map* was originally presented. Assuming linearization of the motion and sensor models and Gaussianity for the underlying probability density functions, the approximate solution to the nonlinear filtering problem was obtained by the Extended Kalman Filter (EKF-SLAM) [2].

Recently, the consistency issues of the EKF-SLAM have attracted the attention of the research community due to their relevance, even with higher priority than computational cost. Dissanayake et al. [3] proved three important convergence properties of the EKF-SLAM: (i) The determinant of any submatrix of the map covariance matrix decreases monotonically as observations are successively made; (ii) in the limit as the number of observations increases, the landmark estimates become fully correlated; and (iii) in the limit, the covariance associated with any single landmark location estimate reaches a lower bound determined only by the initial covariance in the vehicle location estimate at the time of the first sighting of the first landmark.

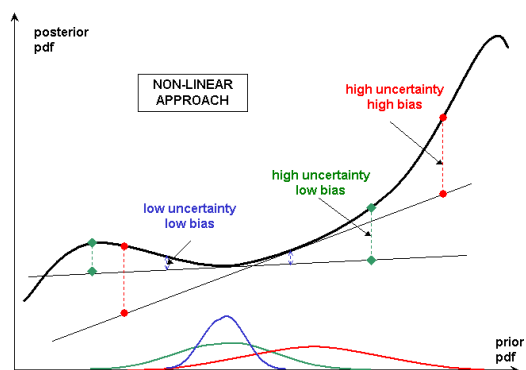


Fig. 1. Influence of the uncertainty of the estimated state-vector in linearization accuracy.

Real EKF-SLAM implementations, however, do not satisfy these properties due to inaccurate approximations of nonlinear transformations. Moreover, for the general nonlinear case it is well known that linearization can lead to filter divergence [2], as has been confirmed in carefully designed experiments [4], [5] which isolate the effects of linearization errors in the EKF-SLAM approach.

The classical EKF linearizes both the motion and sensor models by using a first-order Taylor series expansion around a *working point*, which is the best available estimated state. Therefore: (a) low estimation bias is required to accurately compute the working point, and (b) because the uncertainty of the estimated state-vector is not considered during linearization it must be kept as reduced as possible to constrict the approximation error (Fig. 1). Additionally, Figs. 2(a) and 2(b) describe the influence of observation uncertainty on the Gaussianity assumption of the EKF approach. Clearly, the higher the uncertainty, the worst the Gaussian approximation.

In the last few years, some works have been reported which propose alternative linearization techniques [6], [7] or even non-parametric approaches [8], [9]. Local map sequencing approaches have been broadly studied in the literature [10], [11] for their capabilities of limiting location uncertainty and

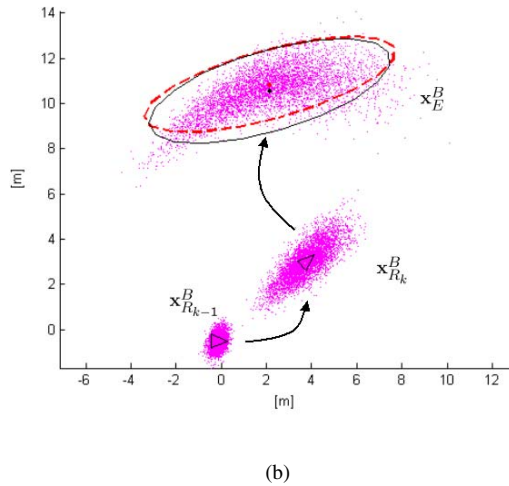
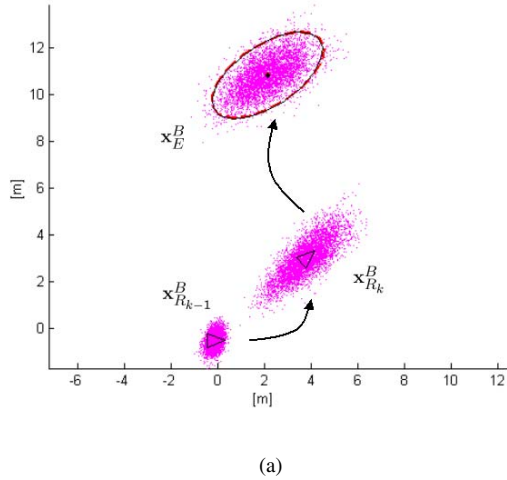


Fig. 2. Influence of observation uncertainty in the Gaussian assumption: (a) low observation noise and (b) high observation noise.

because of their reduced computational cost.

In general, the minimization of linearization errors is based on three main concepts:

- 1) Except during loop-closing, errors and uncertainty increase with the size of the map. Consequently, a bounded map is needed to assure a controlled numerical behavior. A solution consists in building consecutive local maps during exploration.
- 2) Except during loop-closing, computations are made with elements *topologically* close to the robot, so a robot centered representation allows both lower bias and sensor level uncertainties (Fig. 3).
- 3) Any linearized function computed after filter update should be more accurate -working point closer to actual point and lower uncertainty- than the same function computed before the filter update. For example, observations must be taken into account as soon as possible, postponing, whenever possible, any non-reversible lin-

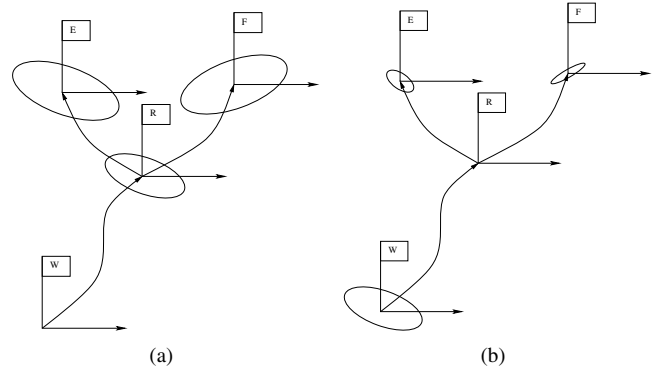


Fig. 3. Comparison of the (a) absolute and (b) robocentric representations. Note that in the robocentric approach, map features close to the robot have lower uncertainty values leading to better approximations of nonlinearities.

earization to the integration of the observation.

These concepts can be summarized in the following idea:

Linearization errors -and filter consistency- are related to the accuracy of the estimated state and its uncertainty in the selected representation.

Based on the previous discussion, we present a robocentric local map sequencing approach which combines the advantages of the local map sequencing approach [11] and the robocentric mapping approach [5], and therefore: (a) bounds location uncertainty within each local map, (b) reduce the computational cost up to constant time in the majority of updates and (c) improves linearization accuracy by updating the map with sensor uncertainty level constraints¹.

The rest of the paper is structured as follows: Section II presents the discrete-time state-space approach to SLAM. Robocentric mapping by using local maps is described in section III. Finally, experimental results validate the proposed approach for both simulated and large-scale outdoor environment.

II. PROBABILISTIC STATE-SPACE GAUSSIAN SLAM

In the probabilistic state-space SLAM, the vehicle R and a set of environment features $\mathcal{F} = \{F_1, \dots, F_n\}$ are represented by a stochastic state vector \mathbf{x}^B with estimated mean $\hat{\mathbf{x}}^B$ and estimated error covariance \mathbf{P}^B :

$$\hat{\mathbf{x}}^B = \begin{bmatrix} \hat{\mathbf{x}}_R^B \\ \hat{\mathbf{x}}_{\mathcal{F}}^B \end{bmatrix}; \mathbf{P}^B = \begin{bmatrix} \mathbf{P}_R^B & \mathbf{P}_{R\mathcal{F}}^B \\ \mathbf{P}_{\mathcal{F}R}^B & \mathbf{P}_{\mathcal{F}}^B \end{bmatrix} \quad (1)$$

where $\hat{\mathbf{x}}_R^B$ is the estimated location of the vehicle with respect to (wrt) a base reference frame B , $\hat{\mathbf{x}}_{\mathcal{F}}^B$ is the estimated location of the features also wrt B , \mathbf{P}_R^B is the estimated error covariance of the location of R , $\mathbf{P}_{\mathcal{F}}^B$ is the estimated error covariance of the location of the features, and finally, $\mathbf{P}_{R\mathcal{F}}^B$ represents the cross-covariance between the different elements of the state vector. Additionally, it is generally assumed that the underlying probability density function is Gaussian, hence, at time step k , $\mathbf{x}_k^B \sim \mathcal{N}(\hat{\mathbf{x}}_k^B, \mathbf{P}_k^B)$.

¹Interestingly, recent research in the field of neuroscience have shown that the human brain also builds an egocentric network of local submaps [12].

When the vehicle moves from position at step $k-1$ to position at step k , the stochastic state vector changes according to a nonlinear motion equation:

$$\mathbf{x}_k^B = \mathbf{f}_k(\mathbf{x}_{k-1}^B, \mathbf{x}_{R_k}^{R_{k-1}}) \quad (2)$$

where the uncertain relative motion $\mathbf{x}_{R_k}^{R_{k-1}}$ is estimated by odometry and assumed to be corrupted by zero mean white Gaussian noise, $\mathbf{v}_k = \mathcal{N}(\mathbf{0}, \mathbf{Q}_k)$.

On-board sensors provide, at time k , the observation \mathbf{z}_k related to the state vector \mathbf{x}_k^B by a nonlinear measurement equation:

$$\mathbf{z}_k = \mathbf{h}_k(\mathbf{x}_k^B, \mathbf{x}_{\mathcal{E}_k}^{R_k}) \quad (3)$$

where $\mathbf{x}_{\mathcal{E}_k}^{R_k}$ represents the set of uncertain observations, wrt R_k , and corrupted by zero mean white Gaussian noise, $\mathbf{w}_k = \mathcal{N}(\mathbf{0}, \mathbf{R}_k)$ independent from the motion noise.

Classical EKF-SLAM suboptimally propagates uncertainty by first-order *analytical* linearization of both the motion (eq. 2) and measurement models (eq. 3). As reported in [4], [5] this approach frequently leads to filter divergence after only a few update steps. The convergence of the filter can be tested by checking the *consistency* of the state estimator [2]: its state estimation error is *unbiased*, i.e. $E[\mathbf{x}_k^B - \hat{\mathbf{x}}_k^B] = \mathbf{0}$ and the actual Mean Square Error matches the filter calculated covariances:

$$E[(\mathbf{x}_k^B - \hat{\mathbf{x}}_k^B)(\mathbf{x}_k^B - \hat{\mathbf{x}}_k^B)^T] = \mathbf{P}_k^B \quad (4)$$

An on-line consistency test is based on the filter *innovation*:

$$E[\mathbf{z}_k - \hat{\mathbf{z}}_k] = \mathbf{0} \quad (5)$$

$$E[(\mathbf{z}_k - \hat{\mathbf{z}}_k)(\mathbf{z}_k - \hat{\mathbf{z}}_k)^T] = \mathbf{P}_{\mathbf{z}\mathbf{z},k} \quad (6)$$

For real applications, the covariance criteria can be relaxed by considering that the estimated covariance bounds the estimated errors, however, a too pessimistic approach would lead to non-informative maps and greater data association ambiguity.

III. ROBOCENTRIC MAPPING

EKF-SLAM using a robot centered representation adopts the previous formulation where the current robot position is considered as the base reference in contrast to the absolute representation where a global reference is used.

Let $\mathbf{x}_{k-1}^{R_{k-1}} \sim \mathcal{N}(\hat{\mathbf{x}}_{k-1}^{R_{k-1}}, \mathbf{P}_{k-1}^{R_{k-1}})$ be the map at time $k-1$ wrt the reference frame R_{k-1} . Being the relative motion of the vehicle $\mathbf{x}_{R_k}^{R_{k-1}}$ independent from the map, it can be added to the state vector as a new uncorrelated feature:

$$\hat{\mathbf{x}}_{k|k-1}^{R_{k-1}} = \begin{bmatrix} \hat{\mathbf{x}}_{k-1}^{R_{k-1}} \\ \hat{\mathbf{x}}_B^{R_{k-1}} \\ \hat{\mathbf{x}}_{\mathcal{F}}^{R_{k-1}} \\ \hat{\mathbf{x}}_{R_k}^{R_{k-1}} \end{bmatrix}; \mathbf{P}_{k|k-1}^{R_{k-1}} = \begin{bmatrix} \mathbf{P}_{k-1}^{R_{k-1}} & \mathbf{P}_{B}^{R_{k-1}} & \mathbf{0} \\ \mathbf{P}_{\mathcal{F}}^{R_{k-1}} & \mathbf{P}_{\mathcal{F}}^{R_{k-1}} & \mathbf{0} \\ \mathbf{0} & \mathbf{0} & \mathbf{Q}_k \end{bmatrix} \quad (7)$$

where B represents the first vehicle location within the current robocentric map. With this approach, during filter update, not only the map but *also* the relative estimated motion would be improved, thus reducing subsequent linearization errors.

The map at time k , $\mathbf{x}_k^{R_{k-1}} \sim \mathcal{N}(\hat{\mathbf{x}}_k^{R_{k-1}}, \mathbf{P}_k^{R_{k-1}})$ is computed by using the classical filter update equations:

$$\begin{aligned} \hat{\mathbf{x}}_k^{R_{k-1}} &= \hat{\mathbf{x}}_{k|k-1}^{R_{k-1}} + \mathbf{K}_k(\mathbf{z}_k - \mathbf{h}_k(\hat{\mathbf{x}}_{k|k-1}^{R_{k-1}})) \\ \mathbf{P}_k^{R_{k-1}} &\simeq (\mathbf{I} - \mathbf{K}_k \mathbf{H}_k) \mathbf{P}_{k|k-1}^{R_{k-1}} \\ \mathbf{K}_k &= \mathbf{P}_{k|k-1}^{R_{k-1}} \mathbf{H}_k^T (\mathbf{H}_k \mathbf{P}_{k|k-1}^{R_{k-1}} \mathbf{H}_k^T + \mathbf{R}_k)^{-1} \end{aligned} \quad (8)$$

where,

$$\mathbf{H}_k = \left. \frac{\partial \mathbf{h}_k}{\partial \mathbf{x}_k^{R_{k-1}}} \right|_{\hat{\mathbf{x}}_{k|k-1}^{R_{k-1}}}$$

Finally, the map at time k in the reference frame of the current robot location R_k is obtained by using the improved relative motion of the vehicle and map feature locations obtained from eq. 8:

$$\hat{\mathbf{x}}_k^{R_k} = \begin{bmatrix} \ominus \hat{\mathbf{x}}_{R_k}^{R_{k-1}} \oplus \hat{\mathbf{x}}_B^{R_{k-1}} \\ \ominus \hat{\mathbf{x}}_{R_k}^{R_{k-1}} \oplus \hat{\mathbf{x}}_{\mathcal{F}}^{R_{k-1}} \end{bmatrix} \quad (9)$$

$$\mathbf{P}_k^{R_k} \simeq [\mathbf{J}_2 \ \mathbf{J}_1] \mathbf{P}_k^{R_{k-1}} \begin{bmatrix} \mathbf{J}_2^T \\ \mathbf{J}_1^T \end{bmatrix} \quad (10)$$

where the Jacobians are given by [13]:

$$\mathbf{J}_1 = \begin{bmatrix} \mathbf{J}_{1\oplus} \{ \ominus \hat{\mathbf{x}}_{R_k}^{R_{k-1}}, \hat{\mathbf{x}}_B^{R_{k-1}} \} \mathbf{J}_{\ominus} \{ \hat{\mathbf{x}}_{R_k}^{R_{k-1}} \} \\ \mathbf{J}_{1\oplus} \{ \ominus \hat{\mathbf{x}}_{R_k}^{R_{k-1}}, \hat{\mathbf{x}}_{\mathcal{F}}^{R_{k-1}} \} \mathbf{J}_{\ominus} \{ \hat{\mathbf{x}}_{R_k}^{R_{k-1}} \} \end{bmatrix}$$

and

$$\mathbf{J}_2 = \begin{bmatrix} \mathbf{J}_{2\oplus} \{ \ominus \hat{\mathbf{x}}_{R_k}^{R_{k-1}}, \hat{\mathbf{x}}_B^{R_{k-1}} \} & \mathbf{0} \\ \mathbf{0} & \mathbf{J}_{2\oplus} \{ \ominus \hat{\mathbf{x}}_{R_k}^{R_{k-1}}, \hat{\mathbf{x}}_{\mathcal{F}}^{R_{k-1}} \} \end{bmatrix}$$

A. Robocentric Map-Joining

Mapping large-scale environments represents an open challenge for the SLAM community. As reported in [11] a computationally attractive approach consists in building a sequence of consecutive uncorrelated local maps and subsequently join them together in a common reference frame resulting in a full correlated global map. This technique limits the number of update steps for each local map, thus, limiting both feature location uncertainties and the effects of linearization errors within each local map. Only the map joining step incurs in $O(n^2)$ computational complexity, where n is the number of features in the global map.

This section formulates the general map joining algorithm by using the robot centered representation. Let the current robocentric local map be given by:

$$\mathcal{M}_{\mathcal{F}}^{R_l} = (\hat{\mathbf{x}}_{\mathcal{F}}^{R_l}, \mathbf{P}_{\mathcal{F}}^{R_l}); \mathcal{F} = \{B_l, F_1, \dots, F_m\}$$

and let the previous robocentric local map be given by:

$$\mathcal{M}_{\mathcal{E}}^{R_{l-1}} = (\hat{\mathbf{x}}_{\mathcal{E}}^{R_{l-1}}, \mathbf{P}_{\mathcal{E}}^{R_{l-1}}); \mathcal{E} = \{B_{l-1}, E_1, \dots, E_n\}$$

Because the two maps have been built sequentially a link between them is established by considering $R_{l-1} = B_l$, i.e. the last updated vehicle position in map $l-1$ coincides with the first vehicle position in map l .

Therefore, the full stochastic map, including all the available features in a common reference frame R_l would be written as:

$$\mathcal{M}_{\mathcal{F}+\mathcal{E}}^{R_l} = (\hat{\mathbf{x}}_{\mathcal{F}+\mathcal{E}}^{R_l}, \mathbf{P}_{\mathcal{F}+\mathcal{E}}^{R_l})$$

where,

$$\hat{\mathbf{x}}_{\mathcal{F}+\mathcal{E}}^{R_l} = \begin{bmatrix} \hat{\mathbf{x}}_{\mathcal{F}}^{R_l} \\ \hat{\mathbf{x}}_{\mathcal{E}}^{R_l} \end{bmatrix} = \begin{bmatrix} \hat{\mathbf{x}}_{\mathcal{F}}^{R_l} \\ \hat{\mathbf{x}}_{R_{l-1}}^{R_l} \oplus \hat{\mathbf{x}}_{\mathcal{E}}^{R_{l-1}} \end{bmatrix} \quad (11)$$

and,

$$\mathbf{P}_{\mathcal{F}+\mathcal{E}}^{R_l} \simeq \begin{bmatrix} \mathbf{P}_{\mathcal{F}}^{R_l} & \mathbf{P}_{\mathcal{F}}^{R_l} \mathbf{J}_1^T \\ \mathbf{J}_1 \mathbf{P}_{\mathcal{F}}^{R_l} & \mathbf{J}_1 \mathbf{P}_{\mathcal{F}}^{R_l} \mathbf{J}_1^T + \mathbf{J}_2 \mathbf{P}_{\mathcal{E}}^{R_{l-1}} \mathbf{J}_2^T \end{bmatrix} \quad (12)$$

with,

$$\mathbf{J}_1 = \begin{bmatrix} \mathbf{J}_{1\oplus} \{ \hat{\mathbf{x}}_{R_{l-1}}^{R_l}, \hat{\mathbf{x}}_{B_{l-1}}^{R_{l-1}} \} & \cdots & \mathbf{0} \\ \vdots & \ddots & \vdots \\ \mathbf{J}_{1\oplus} \{ \hat{\mathbf{x}}_{R_{l-1}}^{R_l}, \hat{\mathbf{x}}_{E_n}^{R_{l-1}} \} & \cdots & \mathbf{0} \end{bmatrix}$$

and,

$$\mathbf{J}_2 = \begin{bmatrix} \mathbf{J}_{2\oplus} \{ \hat{\mathbf{x}}_{R_{l-1}}^{R_l}, \hat{\mathbf{x}}_{B_{l-1}}^{R_{l-1}} \} & \cdots & \mathbf{0} \\ \vdots & \ddots & \vdots \\ \mathbf{0} & \cdots & \mathbf{J}_{2\oplus} \{ \hat{\mathbf{x}}_{R_{l-1}}^{R_l}, \hat{\mathbf{x}}_{E_n}^{R_{l-1}} \} \end{bmatrix}$$

Finally, data association is computed inside the full stochastic map $\mathcal{M}_{\mathcal{F}+\mathcal{E}}^{R_l}$ to remove multiple hypotheses of common features between sets \mathcal{F} and \mathcal{E} . Filter update proceeds according to eq. 8.

IV. EXPERIMENTS

In this section, a series of experiments with synthetic and real outdoor data are presented to validate the proposal.

A. Simulation

In a first set of experiments, we have simulated the exploration of a narrow single-loop corridor of 120 m by a vehicle equipped with odometry and a mid-noise 2D range scanner. Noises are Gaussian distributed in polar coordinates. Filter updates occur once per meter of trajectory. Data association is performed at each step by using the Joint Compatibility algorithm [14] which maximizes innovation consistency. Heading uncertainty has been identified as the critical measure of performance to compare the different approaches due to its direct influence in nonlinear effects in both the motion and the measurement models. A theoretical *lower-bound* for vehicle heading uncertainty has been obtained by computing the linearization Jacobians at the correct linearization point, i.e. with zero error bias (solid lines in figures 4(a) and 4(b)).

Different experiments have been done to analyze the influence of the *choice of representation* in EKF-SLAM. Figure 4(a) describes the results by using an absolute representation, both in the case of building a monolithic map (dotted line) or by joining together a sequence of local maps (dashed line). In both cases, after some update steps, the vehicle heading uncertainty drops below its theoretical lower-bound leading to inconsistency and filter divergence. The use of local maps

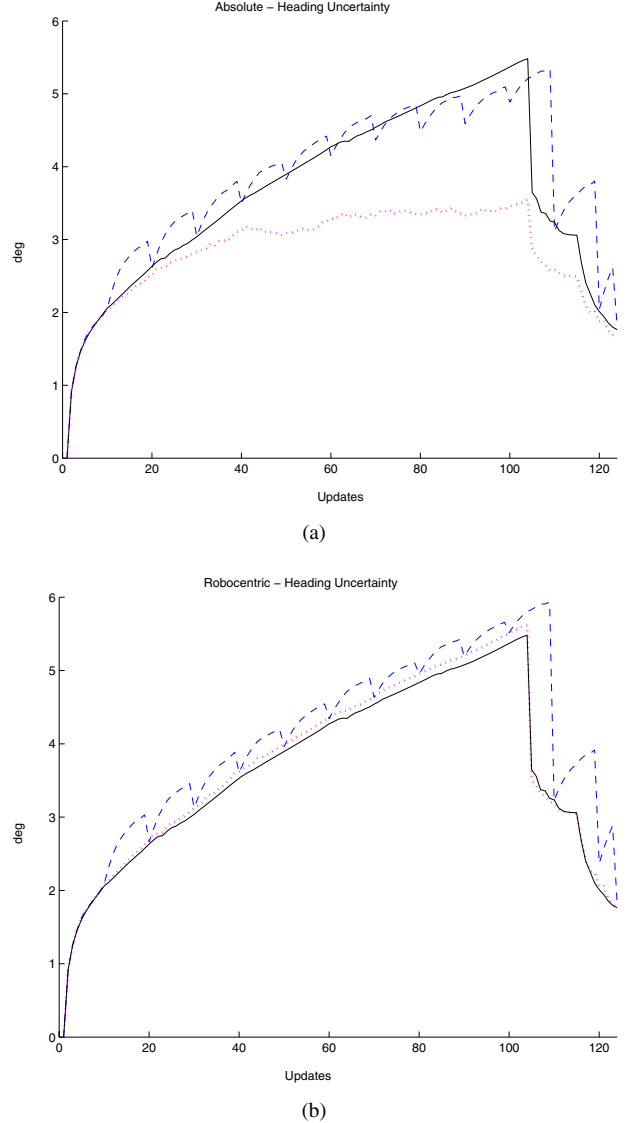


Fig. 4. Heading uncertainty (1σ -bound) using (a) absolute representation and (b) robocentric representation. The figure describes the evolution of the heading uncertainty of the vehicle in the theoretical case (solid lines), when a complete monolithic map is built (dotted lines) and when the global map is built by joining a sequence of local maps (dashed lines).

slightly pushes further in time the appearance of inconsistency, nevertheless, a similar saturation effect is observed in both experiments.

Figure 4(b) shows the improvement in performance obtained by the robocentric representation either using a monolithic (dotted line) or a local map sequencing (dashed line) approach. Note that both results have been transformed back to the base reference frame for ease of comparison with figure 4(a). In this case, filter consistency was satisfied after each update. Computationally, the robocentric local map approach outperformed the monolithic approach at the cost of being slightly more pessimistic during the construction of each local map, from the point of view of the global reference frame. However, within each local map, due to the robocentric representation,

feature location uncertainty was kept down to sensor noise levels. As can be observed in the figure 4(b), the same level of heading uncertainty was computed after joining each local map to the previous global map (at every 10 update steps in this experiment).

B. Outdoor EKF-SLAM

For large-scale outdoor testing experiments, a benchmark dataset has been used [15]. It was collected using a truck (Ackerman vehicle) driving through Victoria Park (Sydney, Australia). On-board sensors provided 2D range scans and odometry (speed and steering). The environment provided a high number of distinguishable landmarks (trees), although with a significant level of spurious observations (e.g. people, cars). Moreover, the bumpy terrain introduced many unexpected odometry perturbations. The complete trajectory was about 3.5 km with several short loops and two critical big loops due to the absence of reliable features in some areas.

Figure 5 shows the the final robocentric map, transformed back to the global frame, and superimposed to a satellite image of the navigated area. Uncertainty ellipses have been drawn for each mapped feature. Data association was, again, performed by using the Joint Compatibility [14] algorithm.

Similarly to the simulation experiments, the vehicle heading uncertainty has been used as the measure of performance to compare the different algorithms. Figure 6 describes its evolution for the navigated outdoor trajectory for the robot centered representation both using a monolithic and a sequence of local maps approaches. The final level of uncertainty for both approaches is comparable after each local map is joined to the previous global map as was observed in the simulation experiments. However, because the local map approach better limits linearization errors within each local map, the final result becomes slightly more pessimistic in comparison to the monolithic approach.

Position uncertainty (i.e. σ_x and σ_y) is represented in fig. 7 for the mapped landmarks after filter update in the final step of the vehicle trajectory for each of the compared algorithms. Due to the greater level of uncertainty when using local maps, as compared to the monolithic case, data association ambiguity grows and therefore the number of false negatives provided by the JC algorithm also increases. Therefore, as observed in the figure, the final number of landmarks is greater in the local map joining approach than in the monolithic approach. Unmatched landmarks means information loss during update.

As observed in figures 7(b) and 7(c), for this particular data set, both local map joining algorithms performed similarly in terms of the final level of position uncertainty of the mapped features. The improvement in the linearization effects of the robocentric representation over the absolute representation, for the chosen size of the local maps, were compensated by the difficulties of data association in correctly find the appropriate matchings.

For a general application, a trade-off between the overall uncertainty level and the computational cost must be established. More accurate and informative maps are obtained by

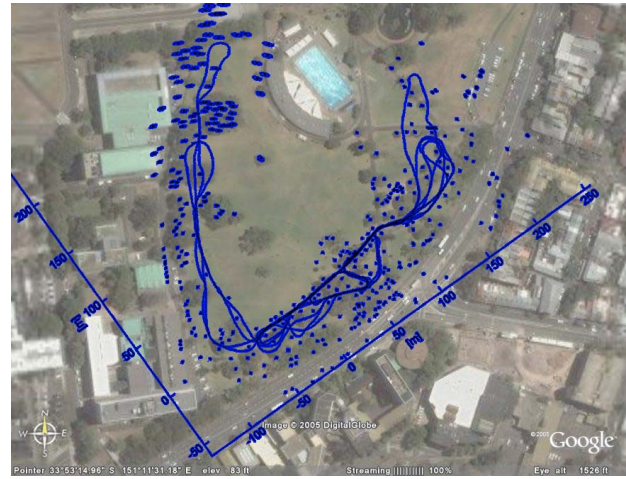


Fig. 5. Trajectory and final feature map superimposed to a satellite image (courtesy of Google Earth <http://earth.google.com>)

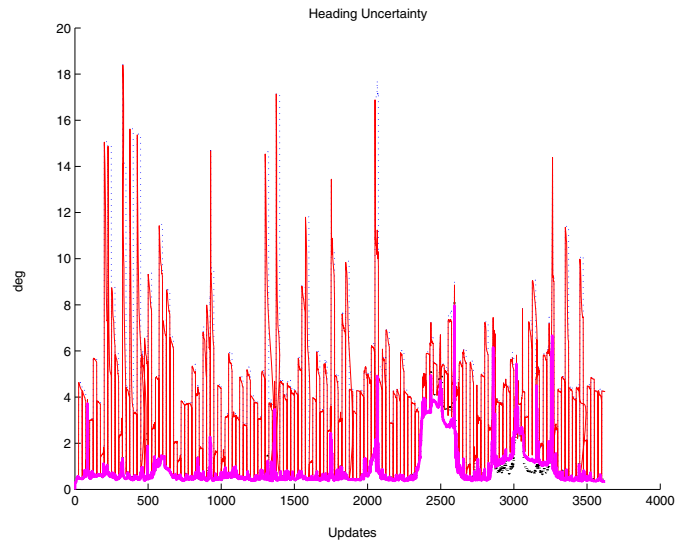


Fig. 6. Heading uncertainty (1σ -bound) for robocentric mapping: Building a monolithic map (solid-thick line) and joining a sequence of local maps (dotted line).

using the monolithic robocentric mapping approach, however, more computationally attractive solutions are obtained when using the robocentric local map joining approach, preserving consistency and convergence. More robust data association algorithms, in the presence of ambiguity, would adequately drive the performance of the latter towards the performance of the former in terms of accuracy and map information.

V. CONCLUSION

In this paper we have presented an algorithm, namely, *robocentric local map sequencing* to minimize the effects of linearization errors in the EKF-SLAM approach. The use of local maps bounds the uncertainty along the vehicle trajectory, and it also provides an efficient solution from the computational point-of-view. The use of the robocentric representation improves linearization accuracy by updating the map with

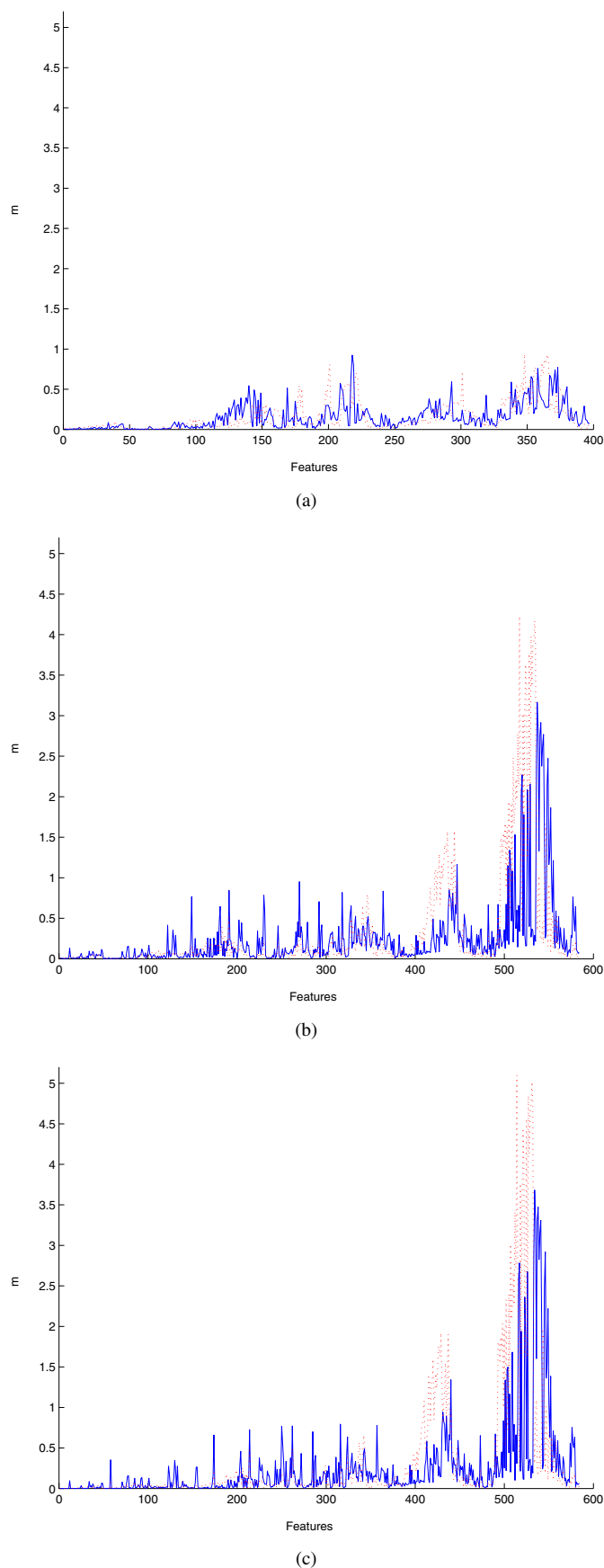


Fig. 7. Position uncertainty (i.e. σ_x , solid-line and σ_y , dotted-line) for mapped landmarks: (a) Robocentric monolithic, (b) Robocentric with local map joining and (c) Absolute local map joining.

sensor uncertainty level constraints. Simulation results have shown that our approach behaves similarly to the ideal case of error-free linearization of both the motion and sensor models. Thus, consistency is greatly improved over the classic EKF-SLAM solution. Large-scale outdoor experiments have validated the approach for a real dataset.

Further work considers the use of alternative linearization techniques, e.g. statistical linearization, within the proposed robocentric representation. Also, new data association algorithms would be required for a robust performance in the presence of ambiguity, clutter and nonlinear models.

ACKNOWLEDGMENT

This research has been funded in part by the Dirección General de Investigación of Spain under project DPI2003-07986.

The authors sincerely thanks to José Guivant and Eduardo Nebot, from the University of Sydney, for making public the Victoria Park dataset.

REFERENCES

- [1] R. Smith, M. Self, and P. Cheeseman, "A Stochastic Map For Uncertain Spatial Relationships," in *Robotics Research, 4th Int. Symposium*, O. Faugeras and G. Giralt, Eds. The MIT Press, 1988, pp. 467–474.
- [2] Y. Bar-Shalom, X. R. Li, and T. Kirubarajan, *Estimation with Applications to Tracking and Navigation*. Wiley InterScience, 2001.
- [3] M. W. M. G. Dissanayake, P. Newman, S. Clark, H. F. Durrant-Whyte, and M. Csorba, "A Solution to the Simultaneous Localization and Map Building (SLAM) Problem," *IEEE Trans. Robot. Automat.*, vol. 17, no. 3, pp. 229–241, 2001.
- [4] S. Julier and J. K. Uhlmann, "A Counter Example to the Theory of Simultaneous Localization and Map Buildin," in *Proc. 2001 IEEE Int. Conf. on Robotics and Automation*, Seoul, Korea, 2001, pp. 4238–4243.
- [5] J. A. Castellanos, J. Neira, and J. D. Tardós, "Limits to the Consistency of EKF-based SLAM," in *5th IFAC Symposium on Intelligent Autonomous Vehicles*, Lisbon, July 2004.
- [6] M. A. Paskin, "Thin Junction Tree Filters for Simultaneous Localization and Mapping," in *Int. Joint Conf. on Artificial Intelligence*, G. Gottlob and T. Walsh, Eds. Morgan Kaufmann, 2003, pp. 1157–1164.
- [7] R. Martinez-Cantin and J. A. Castellanos, "Unscented SLAM for Large-Scale Outdoor Environments," in *IEEE/RSJ Int. Conf. on Intelligent Robots and Systems*, 2005, pp. 328–333.
- [8] A. Doucet and N. de Freitas and K. Murphy and S. Russell, "Rao-Blackwellised Particle Filtering for Dynamic Bayesian Networks," in *Uncertainty in Artificial Intelligence*, 2000.
- [9] S. Thrun, M. Montemerlo, D. Koller, B. Wegbreit, J. Nieto, and E. Nebot, "FastSLAM: An Efficient Solution to the Simultaneous Localization And Mapping Problem with Unknown Data Association," *Journal of Machine Learning Research*, 2004.
- [10] U. Frese, "Treemap: An $O(\log n)$ Algorithm for Simultaneous Localization and Mapping," in *Spatial Cognition IV*, C. Freksa, Ed. Springer Verlag, 2005, pp. 455–476.
- [11] J. D. Tardós, J. Neira, P. M. Newman, and J. J. Leonard, "Robust Mapping and Localization in Indoor Environments using Sonar Data," *Int. J. Robotics Research*, vol. 21, no. 4, pp. 311–330, 2002.
- [12] J. O'Keefe and L. Nadel, *The Hippocampus as a Cognitive Map*. Oxford University Press, 1978.
- [13] J. A. Castellanos and J. D. Tardós, *Mobile Robot Localization and Map Building. A Multisensor Fusion Approach*. Kluwer Academic Publishers, 1999.
- [14] J. Neira and J. D. Tardós, "Data Association in Stochastic Mapping Using the Joint Compatibility Test," *IEEE Trans. Robot. Automat.*, vol. 17, no. 6, pp. 890–897, 2001.
- [15] J. Guivant and E. Nebot, "Optimization of the Simultaneous Localization and Map-Building Algorithm for Real-Time Implementation," *IEEE Trans. Robot. Automat.*, vol. 17, no. 3, pp. 242–257, 2001.